

Article

# Triboelectrification Catalytic Degradation of Organic Pollutants in Water Environment

Haocheng Zhang <sup>†</sup> and Xuefeng Xu <sup>\*,†</sup>

School of Technology, Beijing Forestry University, 35 Qinghua East Road, Beijing 100083, China; zhhch111@bjfu.edu.cn

\* Correspondence: xuxuefeng@bjfu.edu.cn; Tel.: +86-1391-020-5091

† These authors contributed equally to this work.

**Abstract:** With the rapid development of industrialization, more and more organic pollutants are entering the water environment, rendering the treatment of organic pollutants a key issue in protecting it. Therefore, finding a convenient and effective method for degrading organic pollutants in water is of great importance. Triboelectrification is known as the process of charge transfer during the friction process. It is always accompanied by the energy level transition of electrons or holes, making it a potential method for catalytic degradation, which we refer to as triboelectrification catalysis. In this study, a set of experimental equipment was developed. The device is composed of a mechanical system, a control system, and a measurement system that can realize the quantitative measurement of the triboelectrification catalysis under different friction pairs, different loads, and different contact frequencies. Using the developed device, we observed stable triboelectrification catalytic degradation. This study performed triboelectrification catalytic experiments on various organic compounds including methyl orange, rhodamine, and tetracycline. The results revealed that these three organic compounds were degraded by 39%, 15%, and 20%, respectively, within three hours of being under the influence of triboelectrification catalysis. Subsequently, this study conducted triboelectrification catalytic experiments using materials with different triboelectric capacities. This study found that the triboelectric capacity significantly impacted the triboelectrification catalytic degradation rate, providing further evidence for the mechanism of triboelectrification catalysis. Additionally, this study found that SiO<sub>2</sub> and Al<sub>2</sub>O<sub>3</sub>, which also utilize electrons as the primary carrier for triboelectrification, are capable of catalyzing the degradation of a methyl orange solution. Therefore, this study suggests that the triboelectrification catalysis is a versatile and widely applicable method for treating organic pollutants in water. With a broad range of catalyst sources and the ability to effectively degrade various organic pollutants, it shows promise as a solution for the problem of water pollution.

**Keywords:** triboelectrification; triboelectrification catalysis; degradation of organic pollutant; electron transition; methyl orange

**Citation:** Zhang, H.; Xu, X.Triboelectrification Catalytic Degradation of Organic Pollutants in Water Environment. *Catalysts* **2023**, *13*, 936. <https://doi.org/10.3390/catal13060936>

Academic Editor: Mohd Rafatullah

Received: 10 May 2023

Revised: 23 May 2023

Accepted: 24 May 2023

Published: 26 May 2023



**Copyright:** © 2023 by the authors. Licensee MDPI, Basel, Switzerland. This article is an open access article distributed under the terms and conditions of the Creative Commons Attribution (CC BY) license (<https://creativecommons.org/licenses/by/4.0/>).

## 1. Introduction

Industrialization has led to an alarming increase in organic pollutants in the world's bodies of water. For instance, the Songhua River in northeast China has been reported to include over 200 types of organic pollutants, including nitrobenzene, phenol, polycyclic aromatic hydrocarbons, polychlorinated biphenyls, nitrogen-containing organic compounds, benzene compounds, and hydrocarbons [1]. These organic pollutants have serious hazards, many of which have been proven to have strong carcinogenic effects [2]. In addition, they have a strong tendency to accumulate and persist in the environment, often travelling downstream over long distances due to water dynamics after entering the water environment [3]. Due to the widespread distribution and high toxicity of these pollutants, they

cause serious environmental problems, including the clogging of sewage treatment equipment, their adverse effects on aquatic biota, their increased biochemical oxygen demand, the destruction of aquatic ecosystems, and the harm they inflict on aquatic organisms [4].

Most organic pollutants in water are stable and are difficult to degrade under normal conditions, making their degradation in the water environment a challenging task. The two primary methods for degradation are oxidative decomposition and catalytic degradation. The oxidative decomposition method involves adding strong oxidants directly to water to react with organic matter, thereby achieving the purpose of decomposing it [5]. Catalytic degradation mainly includes photocatalysis [6–10] and electrocatalysis [11–13]. During the photocatalytic degradation process, when a catalyst is irradiated with light, the electrons inside the material transition from low to high energy levels, generating electron-hole pairs. These pairs react with hydroxide ions and oxygen molecules in the water, producing hydroxyl radicals  $\cdot\text{OH}$  and superoxide anions  $\text{O}_2^{\cdot-}$ .  $\cdot\text{OH}$  and  $\text{O}_2^{\cdot-}$  are strong oxidizing and reducing agents that decompose the organic matter in water into water and carbon dioxide [14]. The efficiency of photocatalytic degradation is influenced by the choice of material, with degradation rates ranging from 30% to 90%. For instance, the commonly used catalyst ZnS mixed with chitosan-g-poly(acrylamide) material showed a degradation rate of 69% under 4 h of solar light irradiation [15]. However, high-performance catalysts treated with special processes have shown photocatalytic degradation efficiencies towards organic dyes, such as Rhodamine B, that can exceed 90%, and even reach a degradation rate of 99% after a certain period of time in some cases [16–18]. In electrocatalysis, maintaining a certain potential difference between the two electrodes can produce positive and negative charges at the two electrodes. These positive and negative charges also react with water to generate  $\cdot\text{OH}$  and  $\text{O}_2^{\cdot-}$ , playing a similar role to electron-hole pairs [19]. In electrocatalysis, the electrode material plays a significant role in the catalytic degradation efficiency of the solution. Under the coupling effect of photocatalysis, the modified anode of  $\text{BiFeO}_3$  can achieve a degradation rate of about 51.6% for methyl orange [20]. However, when using a composite electrode of  $\text{Sc}_2\text{O}_3$ -magnetite phase titanium ( $\text{Sc}_2\text{O}_3$ -MPT), the degradation rate can reach 90.16% [21].

There are limitations and drawbacks to the current methods of organic degradation. The use of strong oxidants in oxidative decomposition often incurs significant costs and can be harmful to humans. Additionally, the release of these oxidants into water environments can result in secondary pollution [5]. Photocatalysis, on the other hand, requires continuous illumination, and once the illumination stops, the catalytic process ceases immediately. Moreover, its efficiency is limited due to the absorption wavelengths of semiconductor materials being mostly outside of the visible light range. Moreover, once the illumination ceases, the catalytic process also stops. Since catalysis typically employs sunlight as a light source, the efficiency of photocatalysis is limited to some extent [22]. In addition, when light is irradiated into water, refraction and scattering phenomena occur, which reduces the actual energy utilization efficiency of light. Electrocatalysis requires a continuous electric current and has short electrode material lifetimes, resulting in higher costs and reduced degradation efficiency due to unstable current output [5]. Furthermore, when electricity is passed through water, other substances such as water can also be electrolyzed, which further reduces the energy utilization efficiency of electrocatalysis. These constraints limit the widespread application of electrocatalytic oxidation technology in industrial wastewater treatment. Therefore, it is necessary to search for a new, safe, convenient, and efficient catalytic degradation method.

Triboelectrification (TE) refers to the phenomenon of contact surface charging caused by the contact between two objects, and is also known as contact electrification (CE) [23–25]. The charge density generated by triboelectrification is very high, and can even be used to power other components, such as a generator [26,27]. In most cases, triboelectrification is caused by the transfer of electrons between the contact surfaces, which generates electron-hole pairs [28–30]. By utilizing these electron-hole pairs, it is possible to achieve the catalysis of chemical reactions similar to photocatalysis. Previous studies have shown that using

pressure, ultrasound, vibration, and other methods to generate triboelectrification can catalyze certain chemical reactions [31–34]. This process of catalyzing chemical reactions using triboelectrification is called triboelectrification catalysis.

The electron-hole pairs generated by triboelectricity can also be utilized for the catalytic degradation of organic pollutants in water. Experiments have shown that during the magnetic stirring process, friction occurs between polytetrafluoroethylene (PTFE) and  $\text{Ba}_{0.75}\text{Sr}_{0.25}\text{TiO}_3$  (BST) nanoparticles, as well as glass, which mechanically excites electron-hole pairs in the BST nanoparticles, leading to catalytic degradation [35]. An experiment demonstrated that the triboelectrification catalysis of PTFE and BST can achieve a catalytic degradation efficiency of approximately 99% for Rhodamine B after 3 h. In addition, friction between PTFE and  $\text{BiOIO}_3$ , as well as glass vessels, has been found to have a catalytic effect on organic pollutant degradation [36]. According to the experimental results, the triboelectrification catalysis of PTFE and  $\text{BiOIO}_3$  can produce a degradation rate of over 90% for methyl orange solution after 6 h.

Currently, research on triboelectrification catalysis has been limited to the use of nano-sized and submicron-sized particles as catalysts. However, these particle-shaped catalysts are difficult to recover from water, which not only makes it difficult to reuse the catalyst, but also causes water pollution. Block-shaped catalysts are easy to manufacture and convenient to separate from water. Therefore, it is preferable to use block-shaped catalysts for the catalytic degradation of organic pollutants in water. In order to overcome this problem, this paper proposes using block-shaped catalysts to achieve the higher catalytic degradation of organic substances through triboelectrification. However, the triboelectricity efficiency of block-shaped catalysts will inevitably be lower than that of particle-shaped frictional triboelectricity. To increase the efficiency of triboelectrification catalysis, contact electrification is used to increase the amount of triboelectricity. To investigate the triboelectrification catalytic effect of block-shaped catalysts and further study the rules and mechanism of triboelectrification catalysis, a triboelectrification catalysis experimental apparatus was designed. This apparatus achieved quantitative observation of the degradation of organic substances in solution during the frictional contact-separation process by setting parameters such as load size, separation time, and contact times. With this apparatus, preliminary triboelectrification catalysis experiments were conducted, the degradation effect of organic substances by triboelectricity was observed, and a preliminary analysis of the catalytic mechanism was carried out.

In this study, methyl orange (MO), tetracycline (TC), and rhodamine 6G (R6G) were selected as representative organic pollutants for degradation experiments. The molecular weights of these three organic compounds are 296.34, 444.44, and 479.01, respectively. Typically, compounds with molecular weights in the range of 700–800 can be effectively separated from water using specially designed membranes. Therefore, the focus of this research was the catalytic degradation of organic compounds with molecular weights below 700. These three pollutants were chosen due to their molecular weights being close to 300, 400, and 500, respectively. They were also selected for their stability and low toxicity, ensuring their suitability and safety for experimental purposes.

## 2. Results and Discussion

### 2.1. Relationship between Solution Absorbance and Concentration

To verify the accuracy of the solution concentration measurement, we investigated the relationship between the absorbance and concentration of the solution. In the experiment, we first prepared methyl orange solutions of different concentrations (10 mg/L, 20 mg/L, 30 mg/L, and 40 mg/L), and then measured their absorbance at the 435 nm wavelength. The experimental results are shown in Figure 1. The results showed a good linear relationship between the concentration of the methyl orange solution and its absorbance at the 435 nm wavelength (the dashed line in Figure 1 represents the linear fitting of the experimental data points, with a residual square of 0.4256 and a goodness of fit  $R^2$  above 0.99), indicating that

we can use absorbance to calculate the concentration of the solution. The fitting formula is as follows:

$$A = 0.00313 c + 0.01262, \quad (1)$$

According to the calibration results, there is an intercept on the y-axis of the equation. Therefore, when calculating the degradation rate, the intercept needs to be taken into account to make the calculation more accurate.

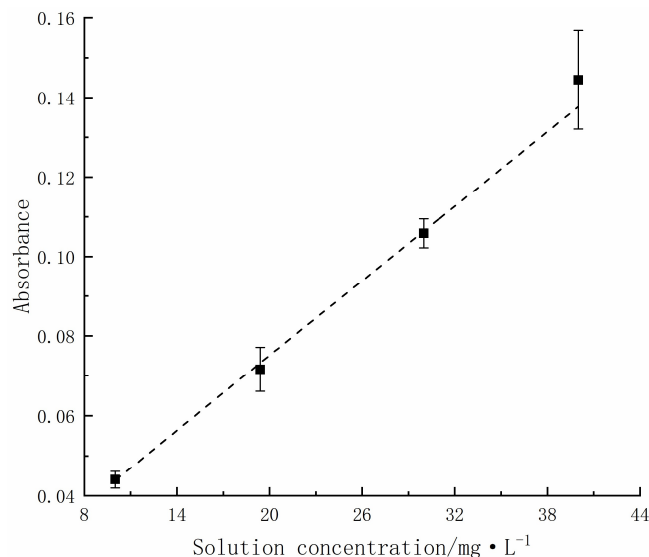


**Figure 1.** Relationship between the absorbance and concentration of methyl orange solution.

## 2.2. Degradation Rate Variation during the Contact Separation Process

To investigate the degradation effect during the contact-separation process of the friction pair, we conducted a triboelectrification catalysis experiment using  $\text{Al}_2\text{O}_3$  as the upper specimen, with  $\text{ZnS}$  as the lower specimen. The experiment was carried out for 1 h, after which the solution was left to stand for 10 min to allow for the uniform diffusion of the solution. Samples were then taken and their absorbance was measured. The change in absorbance of the methyl orange solution over time during the experiment indicated a significant decrease (as shown in Figure 2).

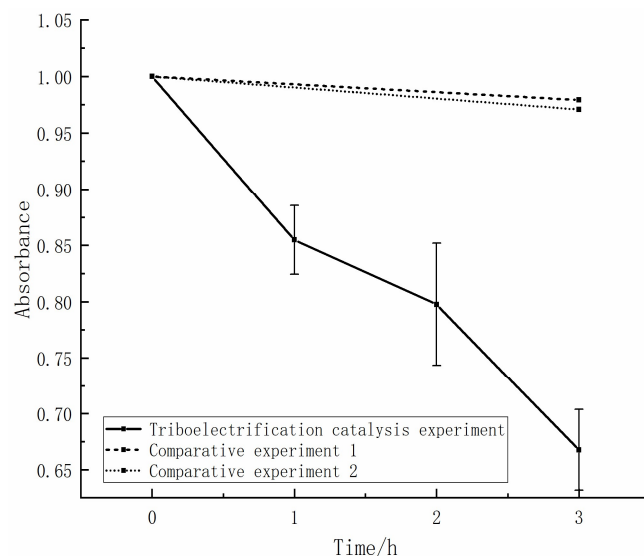


**Figure 2.** Normalization results of the tribological electrocatalysis experiment and the contrast experiment.

To demonstrate that the decrease in solution absorbance is indeed caused by the contact-separation of the friction pair, we conducted two sets of comparative experiments. In the comparative experiment, we still used  $\text{Al}_2\text{O}_3$  and ZnS (used as the upper and lower samples, respectively) in the solution for three hours. In comparative experiment 1, the upper and lower samples were left to stand in the solution for three hours, while in comparative experiment 2, the upper sample was moved up and down but did not come into contact with the lower sample. We measured the absorbance of the solution before and after each comparative experiment and did not observe a significant decrease in solution absorbance (as shown in Figure 2). This indicates that immersing or moving the samples in the solution does not cause a decrease in solution absorbance. Therefore, the observed decrease in solution absorbance during the experiment should be attributed to the contact-separation process between the upper and lower samples.

The experiments demonstrated a direct proportionality between the absorbance of the methyl orange solution and its concentration. Therefore, the change in absorbance during the experiment indicated a change in the solution concentration. As the experiment progressed, the absorbance of the solution continued to decrease, indicating a sustained decrease in concentration and thus the successful degradation of the methyl orange solution. The degradation rate can be calculated using equation (1) based on the changes in absorbance of the solution before and after the experiment. The frictional contact-separation process between the  $\text{Al}_2\text{O}_3$  and ZnS samples achieved a degradation efficiency of over 39% and close to 40%. This degradation efficiency was comparable to or even exceeded the catalytic degradation effect of existing particulate catalysts using triboelectrification catalysis and some other methods such as vibration and temperature. In contrast, the degradation rates of the control experiments were only 2–3%. The small absorbance changes observed in the control experiments were likely due to measurement errors. Based on the above data, we can conclude that the use of block-shaped catalysts for contact electrification can effectively degrade methyl orange in the solution, and the degradation of methyl orange is mainly caused by contact electrification rather than friction between the sample and the solution or the spontaneous degradation of methyl orange. Therefore, triboelectrification catalysis is a feasible approach, and we can utilize it to catalyze the degradation of organic pollutants directly in water.

### 2.3. Degradation Rate at Different Methyl Orange Concentrations

In this study, the triboelectric catalytic performance was tested at different experimental concentrations. According to the experimental results, the catalytic degradation rate was approximately 39% for a concentration of 20 mg/L. However, at a concentration of 40 mg/L, the catalytic degradation rate decreased to approximately 15%, as shown in Figure 3. It was observed that at 40 mg/L concentration, the degradation rate decreased by approximately 61% at 3 h. However, since the concentration doubled, the actual degradation amount should only be slightly lower than that at a concentration of 20 mg/L. Therefore, it can be inferred that the degradation amount may slightly decrease as the concentration increases. In theory, an increase in reactant concentration should accelerate the degradation rate. However, it was observed that the amount of degradation during the same period of time actually decreased. Based on a previous study [37], it was found that methyl orange does not undergo direct degradation into water and carbon dioxide. Instead, it undergoes an initial degradation into shorter chain compounds before further degradation takes place. Furthermore, it was observed that an increase in concentration leads to a higher contact probability between the reactants generated by the mechanically induced catalyst and the methyl orange molecules. As a result, the production of incompletely degraded short chain molecules is significantly enhanced. These short chain molecules exhibit a higher absorbance than water, which leads to a lower degradation rate in the 40 mg/L solution compared to the 20 mg/L solution.

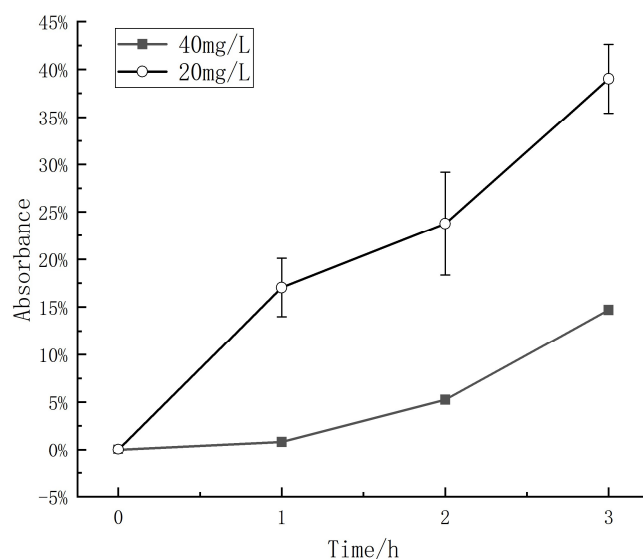


**Figure 3.** The degradation rates of solutions with different concentrations measured over time in triboelectrification catalytic experiments under the same conditions.

#### 2.4. Triboelectrification Catalytic Degradation Effect of Other Organic Pollutants

The Figure 4 demonstrates the use of ZnS and Al<sub>2</sub>O<sub>3</sub> in triboelectrification catalytic experiments on tetracycline and rhodamine. The results showed that this method effectively reduces the solution concentration of both organic compounds in water. According to the formula, the degradation rate of a 20 mg/L methyl orange solution over 3 h can reach 39.09%, and under the same conditions, the degradation rates of rhodamine and tetracycline solutions are approximately 13.76% and 19.95%, respectively. Different types of organic compounds exhibit different degradation rates, and this is likely due to variations in their chemical stability. These findings indicate that triboelectrification catalysis can be used as a widely applicable degradation method for various organic compounds, and is not strictly limited to methyl orange.

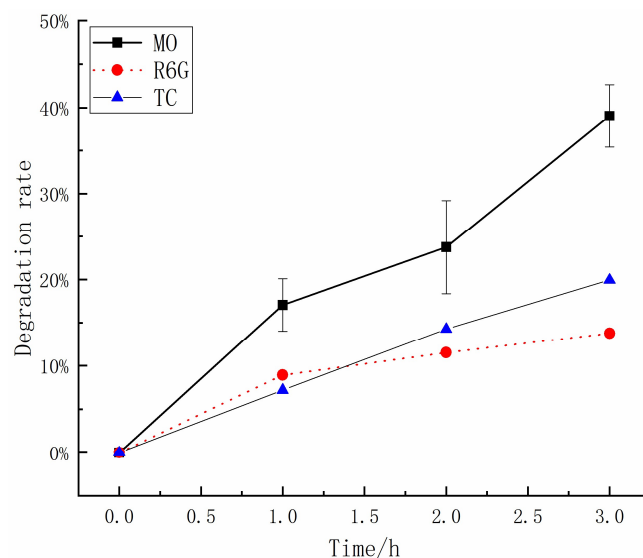


**Figure 4.** The degradation rates of MO, R6G, and TC solutions measured over time in triboelectrification catalytic experiments under the same conditions.

### 2.5. Triboelectrification Catalytic Mechanism

To investigate the degradation mechanism during the contact-separation process, the relationship between the degradation rate and the surface potential generated by triboelectrification catalysis was studied using two types of friction pairs:  $\text{Al}_2\text{O}_3$  (upper)/ $\text{ZnS}$  (lower) and  $\text{Al}_2\text{O}_3$  (upper)/ $\text{CuS}$  (lower). For each friction pair, a 3 h degradation experiment was conducted using a 20 mg/L methyl orange solution as the target, with a load set at approximately 0.196 N, a contact time of 3 s, and a separation time of 5 s. During the experiment, the absorbance of the solution was measured every hour, and the degradation rate at different times was calculated. In addition, the triboelectrification catalysis generated by the friction pairs was measured, and the surface potential changes over time were obtained. The load used in the experiment was approximately 0.196 N. The experimental results are shown in Figure 5.

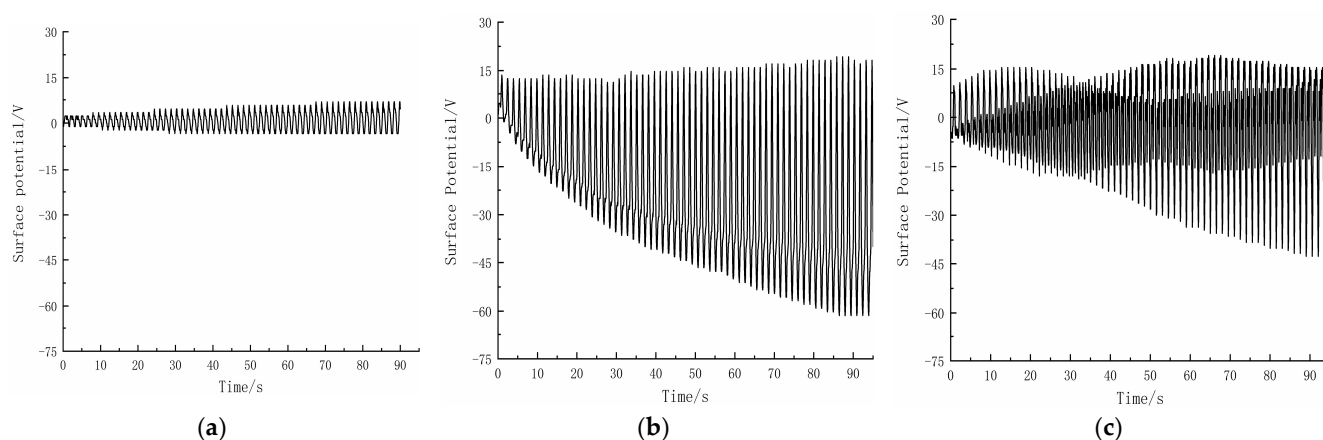


**Figure 5.** The trend diagram of the electric charge of  $\text{Al}_2\text{O}_3$  and different materials calculated by disk-disk sliding friction equipment and the change diagram of the degradation rate of the triboelectrification experiment (a); The effect of triboelectrification between  $\text{Al}_2\text{O}_3$  and  $\text{CuS}$  (b); The effect of triboelectrification between  $\text{Al}_2\text{O}_3$  and  $\text{ZnS}$  (c); The effect of triboelectrification between  $\text{Al}_2\text{O}_3$  and  $\text{SiO}_2$ .

Figure 5a,b show the variation of surface potential with friction time during friction between  $\text{Al}_2\text{O}_3$  and  $\text{CuS}$  and between  $\text{Al}_2\text{O}_3$  and  $\text{ZnS}$ , respectively. The results indicate that the triboelectrification generated by the  $\text{Al}_2\text{O}_3$  and  $\text{CuS}$  pair is relatively small, with a surface potential of only about  $-4$  V, while the  $\text{Al}_2\text{O}_3$  and  $\text{ZnS}$  pair generates a much larger triboelectrification, reaching a surface potential of about  $-60$  V. As shown in Figure 6, the degradation rates of the two friction pairs differed significantly. After 3 h of friction, the  $\text{Al}_2\text{O}_3/\text{CuS}$  friction pair only achieved a degradation rate of about 1%, while the  $\text{Al}_2\text{O}_3/\text{ZnS}$  friction pair achieved a degradation rate of approximately 30%, indicating a significant correlation between degradation and triboelectrification.

The triboelectrification of  $\text{Al}_2\text{O}_3$  and  $\text{SiO}_2$  also exhibit a high frictional charging capacity (as shown in Figure 5c). Therefore, it is theoretically possible to have a degrading effect on methyl orange. The results of the triboelectrification catalytic experiments using  $\text{SiO}_2$  are presented in Figure 6. As the experimental results demonstrate, when  $\text{SiO}_2$  material is used instead of  $\text{ZnS}$  material, it can also achieve a degradation efficiency of about 24.56% on the methyl orange solution. Like  $\text{ZnS}$ , the combination of  $\text{SiO}_2$  and  $\text{Al}_2\text{O}_3$  mainly carries electrons during frictional charging. Hence, it can be inferred that the combination of materials whose primary carriers during frictional charging are electrons could have an excellent catalytic degradation effect on organic compounds.

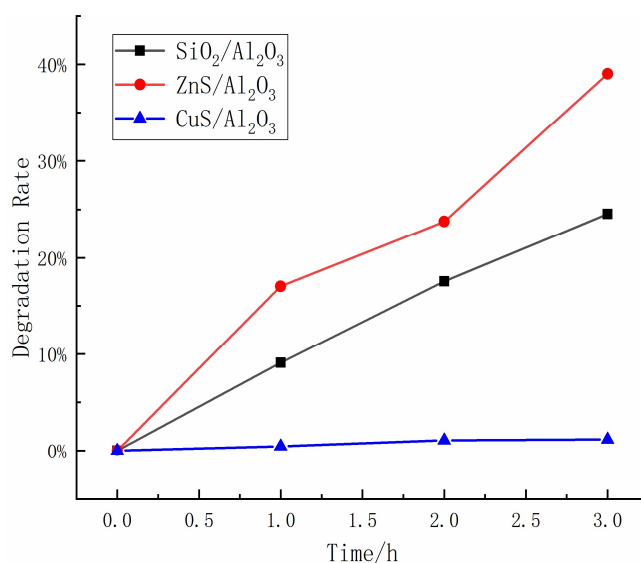


**Figure 6.** Triboelectrification catalytic effect of three materials on the methyl orange solution.

During catalysis, the particles that act as catalysts are typically  $h^+$  or  $OH^-$ , which are generated by the reaction with  $h^+$ . To confirm that the  $h^+$  are responsible for the catalytic degradation in our experiment, we conducted an  $h^+$  trapping experiment with methanol (MA). An amount of 5 mL of MA was added to the solution for the triboelectrification catalytic experiment using ZnS and  $Al_2O_3$  under the same conditions. The results, as shown in the Figure 7, indicated a significant decrease in the degradation rate of the solution after adding MA. This demonstrates a strong relationship between the degradation of the solution and the  $h^+$  generated by triboelectrification during the catalytic process.

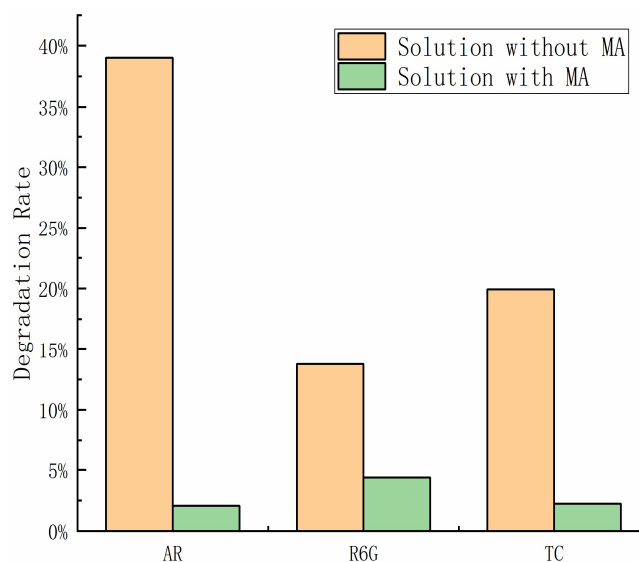


**Figure 7.** Final degradation rate of methyl orange (MO), tetracycline (TC), and rhodamine 6G(R6G) solution in triboelectrification catalytic experiments and methanol capture experiments.

The proposed mechanism for triboelectrification catalytic degradation based on the experimental results can be further explained and improved in the following way (as shown in Figure 8). When the upper and lower samples contact, there an electron transfer occurs (as shown in Figure 8a). When the two samples separate, their surfaces carry charges of opposite polarity (as shown in Figure 8b). During the separation process, the sample surface comes into contact with the solution, and electrons on the sample surface react

with the  $O_2$  dissolved in the water, generating  $O_2^-$ .  $O_2^-$  and holes on the sample surface (maybe  $-OH$  on some other materials), and then react with methyl orange molecules and decompose them into  $H_2O$  and  $CO_2$  (as shown in Figure 8c). As a result, the surface charge of the sample decreases (as shown in Figure 8d) due to the capture of electrons and holes on the sample surface from the organic compound. The upper and lower samples then repeatedly contact and separate, continuously degrading the organic compound molecules.

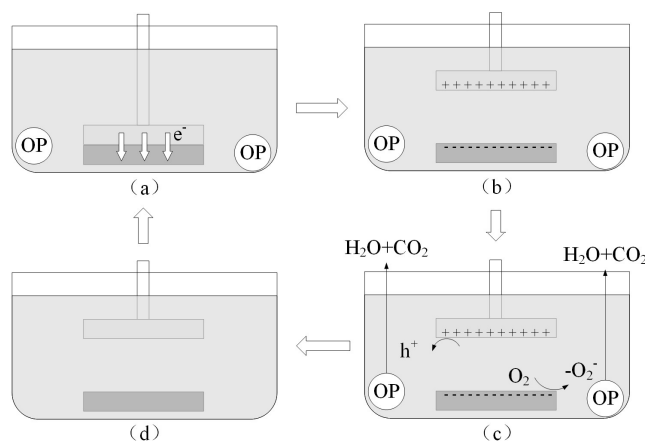


**Figure 8.** (a–d) Degradation mechanism of triboelectrification catalysis.

### 3. Development of the Experimental Device

#### 3.1. Overall Design of the Friction-Starting Electrocatalytic Device

The experimental device is a contact-separation type triboelectrification catalytic instrument. The triboelectricity is generated through the contact-separation process between the upper and lower friction pairs. The triboelectrification catalysis experimental device mainly consists of three parts: a mechanical system, a control system, and a measurement system (shown in Figure 9). To avoid the influence of environmental light, the entire experimental device is placed in a dark box.

- (1) Mechanical system: A stepper motor and screw are used to control the contact and separation between the upper and lower samples.
- (2) Control system: According to the experimental settings, the load size, contact time, separation time, contact frequency, and other parameters are adjusted in real-time during the experiment.
- (3) Measurement system: A tri-axial force sensor is used to convert the force signal into an electrical signal, which is then transmitted to a computer through an amplifier and an acquisition card. The measurement system collects and records the load size and other parameters between the samples in real time.

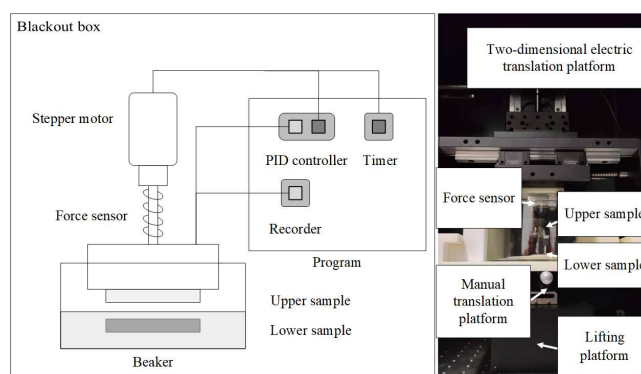


**Figure 9.** Schematic physical diagrams of the triboelectrification catalysis experimental device.

### 3.2. Mechanical System

The mechanical system consists of an electrically-driven two-dimensional translation stage, a manually-driven two-dimensional translation stage, a lifting platform, and upper and lower sample holders (as shown in Figure 7). In the experiment, a disk-shaped sample was used as the friction pair, and the upper and lower sample disks were placed parallel to each other. The organic solution to be degraded was placed in a beaker, and the lower sample disk was fixed in the organic solution with a fixture. The upper sample disk was driven by a stepper motor and a screw rod to achieve contact and separation between the upper and lower sample disks. The electrically-driven and manually-driven two-dimensional translation stages were used to control the horizontal position of the two sample disks and achieve an alignment between them.

### 3.3. Control System

To control the load size and the contact and separation time between the two samples, a control program was developed. The program obtains the normal pressure between the samples and the position of the upper sample in real time, compares them using the experimental settings, and precisely controls the load by controlling the vertical movement of the upper sample.

During the experiment, the control program sends commands to the motion control box to control the stepper motor and drive the upper sample to move through the two-dimensional electric translation platform, thus controlling the load size and the contact and separation time between the upper and lower samples. In addition, the control program has a built-in PID controller to achieve a stable load control between the samples.

### 3.4. Measurement System

In the measurement system, the load between the samples was measured by a three-dimensional force sensor. During the experiment, the program read the electrical signal from the sensor through the acquisition card, converted it into a pressure value, and recorded the load between the two samples in real time. The sensor signal was calibrated, as shown in Figure 10. It can be seen that the load size has a linear relationship with the sensor reading and has good stability.

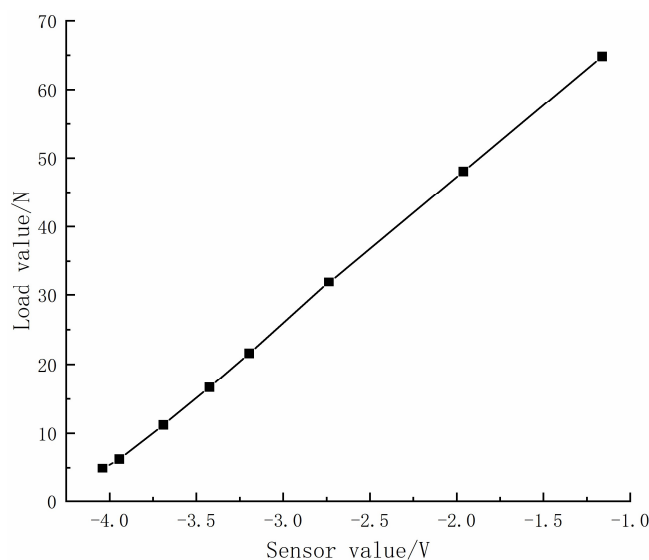


**Figure 10.** The relationship between pressure and sensor reading.

## 4. Materials and Methods

### 4.1. Experimental Materials and Parameters

Friction pair material: In the frictional system, the sample materials consist of aluminum oxide ( $\text{Al}_2\text{O}_3$ ), zinc sulfide ( $\text{ZnS}$ ), silica ( $\text{SiO}_2$ ), and copper sulfide ( $\text{CuS}$ ), with a diameter of 30 mm and a thickness of 2 mm for both the upper and lower samples. All samples used in the experiments were crystal materials obtained from CasCrysTech, CCT (Hangzhou) Technology Co., Ltd. These samples were single crystal targets with a purity of 4 N. Prior to the experiments, the samples were polished to ensure their surfaces were flat, thus ensuring full contact between the friction surfaces.

Organic compound used for degradation: the organic compounds used for degradation were methyl orange (MO), tetracycline (TC), and rhodamine 6G (R6G). The methyl orange solution and the experimental water used for instrument cleaning are both deionized water.

Capturing agent: In this study, methanol (MA) was used as a capturing agent to react with  $\text{h}^+$  in water.

Experimental instruments: The experimental instruments include an Andor spectrometer and a CCD camera.

All experiments and measurements were conducted at room temperature. In the triboelectrification catalytic experiments, the load between the upper and lower samples during contact is approximately 0.196 N.

### 4.2. The Calculation of the Degradation Rate of Organic Pollutants

To analyze the degradation of methyl orange in the experimental solution, this paper first measured the concentration of the methyl orange solution using absorbance experiments. The degradation rate was then calculated by analyzing the changes in the concentration of the methyl orange solution.

The process of measuring the solution's absorbance is shown in Figure 11. Firstly, about 1 mL of the solution is taken and placed into a cuvette. Next, the cuvette is illuminated by a mercury lamp, and the intensity of the light passing through the cuvette containing the solution is measured using a spectrophotometer. The absorbance of the solution can then be calculated from the degree of reduction in the intensity of the mercury lamp light passing through the cuvette. The calculation method is shown below:

$$A = \log \frac{I_0}{I}, \quad (2)$$

In this equation,  $A$  represents the absorbance of the solution to light,  $I$  represents the light intensity after passing through the cuvette containing the solution, and  $I_0$  represents the incident light intensity before entering the cuvette.

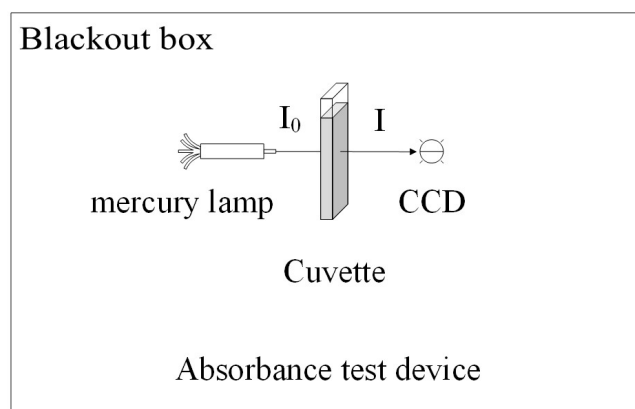


Figure 11. Schematic diagram of the absorbance experimental device.

According to the Beer-Lambert law, the relationship between the absorbance of a solution and its concentration is as follows:

$$A = kbc, \quad (3)$$

In this equation,  $c$  represents the concentration of the solution,  $b$  is the thickness of the solution layer, and  $k$  is a constant value which remains unchanged for the same solute-solvent combination. If  $A_0$  and  $A_1$  are the absorbance values of the methyl orange solution before and after the triboelectrification catalysis experiment, respectively, then the degradation rate of the solution during the experiment can be calculated using the following formula:

$$x = \frac{c_0 - c_1}{c_0} = \frac{\frac{A_0 - q}{kb} - \frac{A_1 - q}{kb}}{\frac{A_0 - q}{kb}} = \frac{A_0 - A_1}{A_0 - q}, \quad (4)$$

In the equation,  $c_0$  represents the initial concentration of the solution,  $q$  represents the intercept in the fitting equation, and  $c_1$  represents the concentration of the solution after degradation.

#### 4.3. Triboelectrification Catalysis Experiment

In the experiment, a 20 mg/L methylene orange solution was used. In each trial, the contact time between the upper and lower sample plates was 3 s, followed by a separation time of 5 s. Each experimental stage lasted for one hour, with the temperature generally maintained at room temperature and a load control of about 0.196 N. We conducted multiple triboelectrification catalytic experiments on the solution under these experimental conditions and recorded the experimental data.

To investigate the catalytic effect of triboelectrification, we conducted experiments to degrade methyl orange through a surface charge generated during the contact-separation process of a friction pair. An amount of 20 mg/L of methyl orange solution was placed in a beaker, and the lower piece of the friction pair was placed stationary in the solution. The upper piece of the friction pair, controlled by a motor, first moved downwards to contact the lower piece. After maintaining a certain contact pressure for a certain time, the upper piece moved upwards again and separated from the lower piece. After the upper piece moved to a certain height and stopped moving, it remained in a stationary state for a certain period of time before moving downwards again. The reciprocating motion of the upper piece moving up and down achieved continuous contact and separation between the two pieces, with one contact-separation cycle between two adjacent contacts.

Figure 12 shows the variation of the contact pressure between the upper and lower specimens with time during a single experiment. In this experiment, the load was set to 0.196 N. Initially, the upper specimen was separated from the lower specimen, and the contact pressure was zero. The upper specimen then moved downward and made contact with the lower specimen, and the contact pressure increased sharply (point a in the figure). After maintaining a contact pressure of approximately 0.196 N for 3 s, the upper specimen began to move upward. As the upper and lower specimens separated, the contact pressure decreased sharply (point b in the figure), and when the specimens were completely separated, the contact pressure was zero. After a 5 s separation, the specimens made contact again (point c in the figure), entering the next contact-separation cycle. In general, this contact separation cycle was repeated 450 times per hour. As the experiment lasted for one hour, the 450 back-and-forth movements caused a vertical displacement of the upper sample. Therefore, when the program detects that the load size is not at the set value, it will adjust the upper sample slightly to restore the load size to the set value.

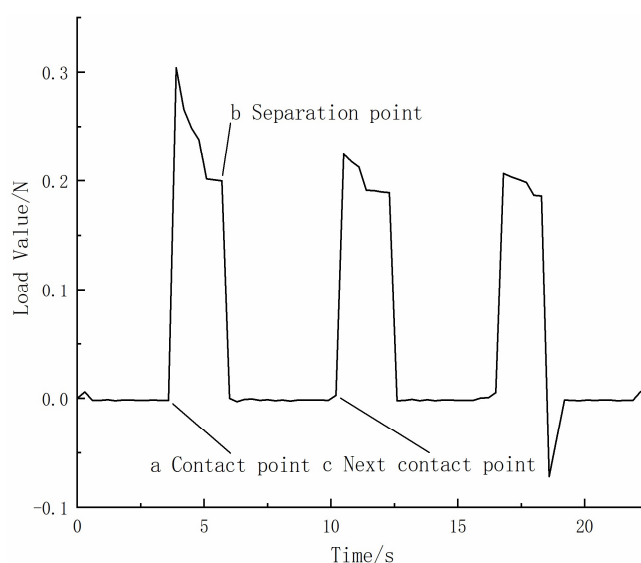


**Figure 12.** Load variation diagram in the experiment.

Before the experiment, a certain volume of the solution was collected and measured to obtain the initial absorbance of the solution. During the experiment, the absorbance of a certain volume of the solution was measured at regular intervals to calculate the degradation rate of the solution using Equation (1) and the initial absorbance. The volume of the collected solution was approximately 1–2 mL, which was negligible compared to the initial volume of the solution (250 mL). Therefore, the collection of the solution would not significantly affect the experimental results.

## 5. Conclusions

The present study designed a triboelectrification catalysis experimental setup that enabled triboelectrification catalysis experiments under different friction pairs, pressures, and contact-separation times. This experimental setup provides an effective means for subsequent triboelectrification catalysis experiments. Through experimentation, the significant degradation of a methyl orange solution was observed, and in comparing experiments, it was demonstrated that the reason for the decrease in the methyl orange solution concentration was the contact-separation process between the samples. These results suggest that block-shaped catalysts can indeed replace particulate catalysts as a method for the catalytic degradation of organic pollutants.

Subsequently, to analyze its degradation mechanism, we investigated the influence of triboelectrification catalysis on the degradation rate, and found a significant correlation between the two. Based on the experimental results, we proposed a reliable triboelectrification catalysis degradation mechanism, which suggested that electron transfer occurs when the upper and lower surfaces are in contact, resulting in the surfaces of the sample being positively or negatively charged. These charges react with water and oxygen to produce strongly redox-active products that can degrade the methyl orange in the solution into water and carbon dioxide, thereby achieving the degradation of methyl orange solution.

We thus conclude that, while block catalysts are not as effective as powdered catalysts in terms of triboelectrification catalysis, they are still capable of catalyzing the degradation of organic pollutants through contact separation alone, achieving a degradation rate of about 39% for methyl orange in just 3 h. Moreover, block catalysts are easily separable from water, which implies that they can be used exclusively for catalytic degradation and practical applications in wastewater treatment. Hence, this study has confirmed the feasibility of using triboelectrification catalysis for organic pollutant degradation. Given the high energy utilization efficiency of triboelectrification catalysis, it has potential as a promising new method that can directly harness the mechanical energy in flowing water for

catalytic degradation. Thus, this study emphasizes the need to focus on triboelectrification catalysis, to promote its recognition, and to further its development.

**Author Contributions:** Conceptualization, H.Z. and X.X.; methodology, H.Z. and X.X.; software, H.Z. and X.X.; validation, H.Z. and X.X.; formal analysis, H.Z. and X.X.; investigation, H.Z. and X.X. resources, H.Z. and X.X.; data curation, H.Z. and X.X.; writing—original draft preparation, H.Z. and X.X.; writing—review and editing, H.Z. and X.X.; visualization, H.Z. and X.X.; supervision, H.Z. and X.X.; project administration, H.Z. and X.X.; funding acquisition, H.Z. and X.X. All authors have read and agreed to the published version of the manuscript.

**Funding:** This research was funded by National Natural Science Foundation of China (No.51527901).

**Data Availability Statement:** The data presented in this study are available in this article.

**Conflicts of Interest:** The authors declare no conflict of interest.

## References

1. Meng, F.; Cheng, P.; Zhang, L.; Wang, Y.; Xue, H. Organic Pollutant Types and Concentration Changes of the Water from Songhua River, China, in 1975–2013. *Water Air Soil Pollut.* **2016**, *227*, 214. [[CrossRef](#)]
2. Yang, L.; Zhu, H.; Liu, Z.; Gao, Z.; Lu, T.; Feng, J.; Sun, H. Health Risk Assessment of Groundwater in the Dawu Water Source Area, Zibo City. *J. Arid Land Resour. Environ.* **2021**, *35*, 106–113.
3. Han, F. Environmental Monitoring Status of Persistent Organic Pollutants in China. *Clean. World* **2022**, *38*, 75–77.
4. Liu, Y.; Wang, L.; Liu, W.; Liu, Q. Research of Organic Pollution's Character in Songhua River. *Environ. Sci. Manag.* **2006**, *31*, 73–75.
5. Song, X. Study on Degradation Methods of Organic Pollutants. *Shanxi Chem. Ind.* **2022**, *42*, 356–357.
6. Yang, J.; Wang, D.; Han, H.; Li, C. Roles of Cocatalysts in Photocatalysis and Photoelectrocatalysis. *Acc. Chem. Res.* **2013**, *46*, 1900–1909. [[CrossRef](#)]
7. Espino-Estévez, M.R.; Fernández-Rodríguez, C.; González-Díaz, O.M.; Araña, J.; Espinós, J.P.; Ortega-Méndez, J.A.; Doña-Rodríguez, J.M. Effect of TiO<sub>2</sub>-Pd and TiO<sub>2</sub>-Ag on the Photocatalytic Oxidation of Diclofenac, Isoproturon and Phenol. *Chem. Eng. J.* **2016**, *298*, 82–95. [[CrossRef](#)]
8. Dai, B.; Zhao, W.; Huang, H.; Li, S.; Yang, G.; Wu, H.; Sun, C.; Dennis, Y.C.L. Constructing an Ohmic Junction of Copper@ Cuprous Oxide Nanocomposite with Plasmonic Enhancement for Photocatalysis. *J. Colloid Interface Sci.* **2022**, *616*, 163–176. [[CrossRef](#)]
9. Lou, W.; Wang, L.; Dong, S.; Cao, Z.; Sun, J.; Zhang, Y. A Facile Synthesis of Bismuth-Iron Bimetal MOF Composite Silver Vanadate Applied to Visible Light Photocatalysis. *Opt. Mater.* **2022**, *126*, 112168. [[CrossRef](#)]
10. Zeng, Y.; Lu, D.; Kondamareddy, K.K.; Wang, H.; Wu, Q.; Fan, H.; Wang, Q.; Zhang, B.; Xie, L.; Zhang, Y. Enhanced Visible Light Photocatalysis and Mechanism Insight for Novel Z-Scheme MoS<sub>2</sub>/Ag<sub>2</sub>S/AgVO<sub>x</sub> Ternary Heterostructure with Fast Interfacial Charges Transfer. *J. Alloys Compd.* **2022**, *908*, 164642. [[CrossRef](#)]
11. He, Z.; Liu, S.; Zhong, Y.; Chen, D.; Hao, Q. Preparation of BiPO<sub>4</sub>/Graphene Photoelectrode and Its Photoelectrocatalytic Performance. *Chin. J. Catal.* **2020**, *41*, 302–311. [[CrossRef](#)]
12. Ai, L.; Luo, Y.; Huang, W.; Tian, Y.; Jiang, J. Cobalt/Cerium-Based Metal-Organic Framework Composites for Enhanced Oxygen Evolution Electrocatalysis. *Int. J. Hydrogen Energy* **2022**, *47*, 12893–12902. [[CrossRef](#)]
13. Zeng, L.; He, Z.; Luo, Y.; Xu, J.; Chen, J.; Wu, L.; Huang, P.; Xu, S. A Simple g-C<sub>3</sub>N<sub>4</sub>/TNs Heterojunction for Improving the Photoelectrocatalytic Degradation of Methyl Orange. *J. Electrochem. Soc.* **2021**, *168*, 116520. [[CrossRef](#)]
14. Li, H.; Sun, B.; Gao, T.; Li, H.; Ren, Y.; Zhou, G. Ti<sub>3</sub>C<sub>2</sub> MXene co-catalyst assembled with mesoporous TiO<sub>2</sub> for boosting photocatalytic activity of methyl orange degradation and hydrogen production. *Chin. J. Catal.* **2022**, *43*, 461–471. [[CrossRef](#)]
15. Pathania, D.; Gupta, D.; Al-Muhtaseb, A.H.; Sharma, G.; Kumar, A.; Naushad, M.; Ahamad, T.; Alshehri, S.M. Photocatalytic degradation of highly toxic dyes using chitosan-g-poly(acrylamide)/ZnS in presence of solar irradiation. *J. Photochem. Photobiol. A Chem.* **2016**, *329*, 61–68. [[CrossRef](#)]
16. Saeed, M.; Al-Saeed, F.A.; Altaf, M.; Alahmari, S.D.; Bokhari, T.H.; Bajaber, M.A.; Khan, I.; Ahmed, A.E. Synthesis of a visiblelight-driven Ag<sub>2</sub>O-Co<sub>3</sub>O<sub>4</sub> Z-scheme photocatalyst for enhanced photodegradation of a reactive yellow dye. *New J. Chem.* **2022**, *46*, 23297–23304. [[CrossRef](#)]
17. Saeed, M.; Khan, I.; Adeel, M.; Akram, N.; Muneer, M. Synthesis of a CoO-ZnO photocatalyst for enhanced visible-light assisted photodegradation of methylene blue. *New J. Chem.* **2022**, *46*, 2224–2231. [[CrossRef](#)]
18. Saeed, M.; Alwadai, N.; Ben Farhat, L.; Baig, A.; Nabgan, W.; Iqbal, M. Co<sub>3</sub>O<sub>4</sub>-Bi<sub>2</sub>O<sub>3</sub> heterojunction: An effective photocatalyst for photodegradation of rhodamine B dye. *Arab. J. Chem.* **2022**, *15*, 103732. [[CrossRef](#)]
19. Zhang, W.; Ma, X.; Zou, S.; Cai, W. Recent advances in glycerol electrooxidation on Pt and Pd: From reaction mechanisms to catalytic materials. *J. Electrochem.* **2021**, *27*, 233–256.
20. Zhang, X.; Song, X.; Lu, Z.; Chen, A.; Li, C. Anode modified by BiFeO<sub>3</sub> and application in resourceful treatment of salty organic wastewater. *Micro Nano Lett.* **2019**, *14*, 683–687. [[CrossRef](#)]

21. Bai, H.; He, P.; Chen, J.; Liu, K.; Lei, H.; Dong, F.; Zhang, X.; Li, H. Fabrication of  $\text{Sc}_2\text{O}_3$ -magneli phase titanium composite electrode and its application in efficient electrocatalytic degradation of methyl orange. *Appl. Surf. Sci.* **2017**, *401*, 218–224. [[CrossRef](#)]
22. Hong, Y.; Ma, J.; Wu, Z.; Ying, J.; You, H.; Jia, Y. Piezo-electrochemical coupling of  $\text{AgNbO}_3$  Piezoelectric Nanomaterials. *Acta Phys. Sin.* **2018**, *67*, 202–208.
23. Li, G.; Yang, S.; Xing, P.; Liu, T.; Gao, H.; Song, Y.; Zhang, H. Experimental Investigation of Triboelectrification Behaviour in the Friction Process. *Lubricants* **2022**, *10*, 180. [[CrossRef](#)]
24. Mariappan, V.K.; Krishnamoorthy, K.; Pazhamalai, P.; Manoharan, S.; Kim, S. Decoupling Contact and Rotary Triboelectrification vs Materials Property: Toward Understanding the Origin of Direct-Current Generation in TENG. *ACS Appl. Mater. Interfaces* **2022**, *14*, 34593–34602. [[CrossRef](#)]
25. Wang, K.; Qiu, Z.; Wang, J.; Liu, Y.; Chen, R.; An, H.; Park, J.H.; Suk, C.H.; Wu, C.; Lin, J.; et al. Effect of Relative Humidity on the Enhancement of the Triboelectrification Efficiency Utilizing Water Bridges between Triboelectric Materials. *Nano Energy* **2022**, *93*, 106880. [[CrossRef](#)]
26. Xu, C.; Zi, Y.; Wang, A.C.; Zou, H.; Dai, Y.; He, X.; Wang, P.; Wang, Y.; Feng, P.; Li, D.; et al. On the Electron-Transfer Mechanism in the Contact-Electrification Effect. *Adv. Mater.* **2018**, *30*, 1706790. [[CrossRef](#)]
27. Niu, S.; Wang, S.; Lin, L.; Liu, Y.; Zhou, Y.; Hu, Y.; Wang, Z. Theoretical Study of Contact-Mode Triboelectric Nanogenerators as an Effective Power Source. *Energy Environ. Sci.* **2013**, *6*, 3576–3583. [[CrossRef](#)]
28. Matsusaka, S.; Maruyama, H.; Matsuyama, T.; Ghadiri, M. Triboelectric Charging of Powders: A Review. *Chem. Eng. Sci.* **2010**, *65*, 5781–5807. [[CrossRef](#)]
29. Matsuyama, T.; Yamamoto, H. Impact charging of particulate materials. *Chem. Eng. Sci.* **2005**, *61*, 2230–2238. [[CrossRef](#)]
30. Li, S.; Zhou, Y.; Zi, Y.; Zhang, G.; Wang, Z. Excluding contact electrification in surface potential measurement using Kelvin probe force microscopy. *ACS Nano* **2016**, *10*, 2528–2535. [[CrossRef](#)]
31. Chen, L.; Jia, Y.; Zhao, J.; Ma, J.; Wu, Z.; Yuan, G.; Cui, X. Strong piezocatalysis in barium titanate/carbon hybrid nanocomposites for dye wastewater decomposition. *J. Colloid Interface Sci.* **2021**, *586*, 758–765. [[CrossRef](#)] [[PubMed](#)]
32. Sun, C.; Guo, X.; Ji, R.; Hu, C.; Liu, L.; Fang, L.; Cheng, Z.; Luo, N. Strong Tribocatalytic Dye Degradation by Tungsten Bronze  $\text{Ba}_4\text{Nd}_2\text{Fe}_2\text{Nb}_8\text{O}_{30}$ . *Ceram. Int.* **2021**, *47*, 5038–5043. [[CrossRef](#)]
33. You, H.; Ma, X.; Wu, Z.; Fei, L.; Chen, X.; Yang, J.; Liu, Y.; Jia, Y.; Li, H.; Wang, F.; et al. Piezoelectrically/Pyroelectrically-Driven Vibration/Cold-Hot Energy Harvesting for Mechano-/Pyro-bi-catalytic Dye Decomposition of  $\text{NaNbO}_3$  Nanofibers. *Nano Energy* **2018**, *52*, 351–359. [[CrossRef](#)]
34. Ma, J.; Ren, J.; Jia, Y.; Wu, Z.; Chen, L.; Haugen, N.O.; Huang, H.; Liu, Y. High efficiency bi-harvesting light/vibration energy using piezoelectric zinc oxide nanorods for dye decomposition. *Nano Energy* **2019**, *62*, 376–383. [[CrossRef](#)]
35. Li, P.; Wu, J.; Wu, Z.; Jia, Y.; Ma, J.; Chen, W.; Zhang, L.; Yang, J.; Liu, Y. Strong tribocatalytic dye decomposition through utilizing triboelectric energy of barium strontium titanate nanoparticles. *Nano Energy* **2019**, *63*, 103832. [[CrossRef](#)]
36. Lei, H.; Wu, M.; Mo, F.; Ji, S.; Dong, X.; Wu, Z.; Gao, J.; Yang, Y.; Jia, Y. Tribo-catalytic degradation of organic pollutants through bismuth oxyiodate triboelectrically harvesting mechanical energy. *Nano Energy* **2020**, *78*, 105290. [[CrossRef](#)]
37. Wu, Q.; Zhou, Y.; Feng, J. Study of  $\text{TiO}_2$  photocatalytic degradation process of methyl orange using two-dimensional correlation spectroscopy. In *18th National Conference on Molecular Spectroscopy*; Chinese Optical Society, Chinese Chemical Society; Peking University Press: Beijing, China, 2014; p. 2.

**Disclaimer/Publisher’s Note:** The statements, opinions and data contained in all publications are solely those of the individual author(s) and contributor(s) and not of MDPI and/or the editor(s). MDPI and/or the editor(s) disclaim responsibility for any injury to people or property resulting from any ideas, methods, instructions or products referred to in the content.